

High-frequency magnetic properties and core loss of carbonyl iron composites with easy plane-like structures

Guo-Wu Wang(王国武), Chun-Sheng Guo(郭春生), Liang Qiao(乔亮), Tao Wang(王涛), and Fa-Shen Li(李发伸)
Citation: Chin. Phys. B, 2021, 30 (**2**): 027504. DOI: 10.1088/1674-1056/abc15c
Journal homepage: http://cpb.iphy.ac.cn; http://iopscience.iop.org/cpb

What follows is a list of articles you may be interested in

Table-like shape magnetocaloric effect and large refrigerant capacity in dual-phase HoNi/$HoNi_2$ composite

Dan Guo(郭丹), Yikun Zhang(张义坤)†, Yaming Wang(王雅鸣), Jiang Wang(王江), and Zhongming Ren(任忠鸣)‡
Chin. Phys. B, 2020, 29 (**10**): 107502. DOI: 10.1088/1674-1056/aba9be

High permeability and bimodal resonance structure of flaky soft magnetic composite materials

Xi Liu(刘曦), Peng Wu(吴鹏), Peng Wang(王鹏), Tao Wang(王涛), Liang Qiao(乔亮), Fa-Shen Li(李发伸)
Chin. Phys. B, 2020, 29 (**7**): 077506. DOI: 10.1088/1674-1056/ab8c3b

High pressure synthesis and characterization of the pyrochlore $Dy_2Pt_2O_7$: A new spin ice material

Qi Cui(崔琦), Yun-Qi Cai(蔡云麒), Xiang Li(李翔), Zhi-Ling Dun(顿志凌), Pei-Jie Sun(孙培杰), Jian-Shi Zhou(周建十), Hai-Dong Zhou(周海东), Jin-Guang Cheng(程金光)
Chin. Phys. B, 2020, 29 (**4**): 047502. DOI: 10.1088/1674-1056/ab7b58

Dynamical anisotropic magnetoelectric effects at ferroelectric/ferromagnetic insulator interfaces

Yaojin Li(李耀进), Vladimir Koval, Chenglong Jia(贾成龙)
Chin. Phys. B, 2019, 28 (**9**): 097501. DOI: 10.1088/1674-1056/ab37f7

Enhanced soft magnetic properties of iron powders through coating MnZn ferrite by one-step sol-gel synthesis

Dong Liu(刘冬), Shanmin Gao(高善民), Rencheng Jin(金仁成), Feng Wang(王峰), Xiaoxiao Chu(初晓晓), Taiping Gao(高太平), Yubao Wang(王玉宝)
Chin. Phys. B, 2019, 28 (**5**): 057503. DOI: 10.1088/1674-1056/28/5/057503

High-frequency magnetic properties and core loss of carbonyl iron composites with easy plane-like structures*

Guo-Wu Wang(王国武)[1], Chun-Sheng Guo(郭春生)[2], Liang Qiao(乔亮)[1], Tao Wang(王涛)[1,3,†], and Fa-Shen Li(李发伸)

[1] *Key Laboratory for Magnetism and Magnetic Materials of MOE, Lanzhou University, Lanzhou* 730000, *China*
[2] *Guangzhou Newlife Magnet Electricity Co., Ltd., Guangzhou* 511356, *China*
[3] *Key Laboratory of Special Function Materials and Structure Design (Ministry of Education), Lanzhou University, Lanzhou* 730000, *China*

(Received 23 August 2020; revised manuscript received 18 September 2020; accepted manuscript online 15 October 2020)

To fully release the potential of wide bandgap (WBG) semiconductors and achieve high energy density and efficiency, a carbonyl iron soft magnetic composite (SMC) with an easy plane-like structure is prepared. Due to this structure, the permeability of the composite increases by 3 times (from 7.5 to 21.5) at 100 MHz compared with to the spherical carbonyl iron SMC, and the permeability changes little at frequencies below 100 MHz. In addition, the natural resonance frequency of the composite shifts to higher frequencies at 1.7 GHz. The total core losses of the composites at 10, 20, and 30 mT are 80.0, 355.3, and 810.7 mW/cm^3, respectively, at 500 kHz. Compared with the spherical carbonyl iron SMC, the core loss at 500 kHz is reduced by more than 60%. Therefore, this kind of soft magnetic composite with an easy plane-like structure is a good candidate for unlocking the potential of WBG semiconductors and developing the next-generation power electronics.

Keywords: soft magnetic composite, high frequency magnetic property, power electronic, core loss

PACS: 75.30.Cr, 75.30.Gw, 75.40.Gb, 76.20.+q **DOI:** 10.1088/1674-1056/abc15c

1. Introduction

Power electronic equipment (such as sensors, transformers, and motors) is widely used in the energy field, including the generation, transmission, and conversion of electrical energy. However, problems such as severe heating, low energy density, and large size and mass result in high energy loss and low energy conversion efficiency of power electronic devices.[1–5] For example, according to the International Energy Agency, if all industrial motors were driven by a new generation of power electronic devices, more than 300×10^6 kWh of electricity would be saved globally by 2030.[1,6] Therefore, to reduce the electricity consumption throughout industrial society, the next-generation power electronics must meet the requirements of high energy density, high energy conversion efficiency, miniaturization, and lightness. According to power electronics, increasing the operating frequency can reduce the size of the devices' inductance and capacitance while keeping the ripple voltage constant.[1] Therefore, developing high-frequency soft magnetic materials (SMMs) that can work efficiently at high frequencies is the key to producing energy electronic devices with high energy density. The development of wide bandgap (WBG) semiconductors (SiC and GaN) makes it possible for power electronic devices to work at higher frequencies with higher energy density and energy conversion efficiency.[7] However, the SMMs needed for power electronic devices remain lacking.

At present, due to the advantages of high permeability, low core loss, and cheap price, soft ferrites, such as MnZn, NiZn, and NiZnCu ferrites, almost monopolize the SMMs in all power electronic devices.[8–16] However, these materials have an unsurmountable defect that their low saturation magnetization and operating frequency cannot meet the requirements of the next-generation power electronics. SMMs such as carbonyl iron, FeNi and FeSi have a natural resonance frequency up to GHz and can maintain a permeability that does not decrease with frequency.[17–23] Unfortunately, the permeability of traditional soft magnetic composites (SMCs) is very low (usually less than 10), which results in high core loss when used at high frequencies. Therefore, to fully unlock the potential of WBG semiconductors and meet the needs of the next-generation power electronics, SMMs must have high operating frequencies (over 100 MHz) and simultaneously have a permeability as high as possible.[1] However, due to the Snoek limit, traditional soft magnetic materials cannot simultaneously achieve a high natural resonance frequency and high magnetic permeability. The Snoek limit[24,25] can be expressed as follows:

$$(\mu_i - 1) f_r = \frac{2}{3}\gamma' M_s, \tag{1}$$

where μ_i is the initial permeability, f_r is the natural resonance frequency, γ is the gyromagnetic ratio, and M_s is the saturation magnetization. According to Eq. (1), in a certain material,

*Project supported by the National Natural Science Foundation of China (Grant Nos. 11574122 and 51731001) and Joint Fund of Equipment Pre-Research and Ministry of Education, China (Grant No. 6141A02033242).

†Corresponding author. E-mail: wtao@lzu.edu.cn

© 2021 Chinese Physical Society and IOP Publishing Ltd

its $(\mu_i - 1) f_r$ value is constant, which means that high natural resonance frequency and high permeability cannot be satisfied simultaneously. This is the fundamental reason for restricting the use of SMMs at high frequencies. Therefore, to fully unlock the potential of WBG semiconductors and meet the needs of the next generation of power electronic devices, the Snoek limit must be exceeded. For easy-plane SMMs, the relationship between permeability and natural resonance frequency is as follows:[26]

$$(\mu_i - 1) f_r = \frac{2}{3}\gamma' M_s \sqrt{\frac{H_\theta}{H_\varphi}}, \tag{2}$$

where H_θ and H_φ are out-of-plane and in-plane anisotropic fields, respectively. Since $H_\theta \gg H_\varphi$, the easy-plane material will have a higher $(\mu_i - 1) f_r$ value and thus a higher permeability at higher frequencies.

In this study, we prepare a kind of easy-plane-like carbonyl iron composite using high-aspect-ratio flaky carbonyl iron (HAR-FCI) particles. On the one hand, since $H_\theta \gg H_\varphi$, this material can effectively break through the Snoek limit and achieve higher permeability at higher frequencies. On the other hand, HAR-FCI particles can effectively inhibit the skin effect and reduce eddy current loss. Combined with these two advantages, carbonyl iron composites with easy-plane-like structure can be a good candidate material to fully unlock the potential of WBG semiconductors and meet the requirements of the next-generation power electronics.

2. Experiment

In experiment, HAR-FCI particles were obtained by planetary ball milling. ZnO ball grinding balls ($d = 5$ mm) were used, and the ratio of ball to powder was 25:1. The rotation speed and time were 350 r/min and 8 h, respectively. We took 50 mL anhydrous ethanol used on each 4 g carbonyl iron powder during the ball milling process. Then 1 g of raw carbonyl iron (R-SCI) and 1 g of HAR-FCI were uniformly mixed with 0.13 g of polyurethane (PU) in an ultrasonic environment, respectively. Here, a certain amount of acetone was used to dissolve the PU. After completely mixing, the HAR-FCI mixture was rotated for 10 min at a magnetic field of 1 T to ensure that all HAR-FCI particles were aligned parallel to a certain plane. Both mixtures were kept at 60 °C for 10 h to dry the excess acetone in the mixture. After complete drying, it was pressed at a pressure of 4 MPa to form a ring with an outer diameter of 15 mm, an inner diameter of 7 mm, and a thickness of 5 mm, which were respectively labeled as SCI/PU and FCI/PU. Figure 1 presents a schematic diagram of the composites.

The morphology of the R-SCI and HAR-FCI particles was observed with a scanning electron microscope (SEM, Hitachi S-4800). The phase structure was characterized by powder x-ray diffraction (XRD, Philips X'Pert PRO) with Cu $K\alpha$ radiation ($\lambda = 0.15418$ nm). The composites' static magnetic properties were measured at room temperature using a vibrating sample magnetometer (VSM, Lake Shore 7304). The magnetic moment orientation of the as-milled composites was characterized by the room temperature transmission Mössbauer spectra. In the transmission geometry, the incident γ-ray was parallel to the axis of the oriented disk. The permeability of the composites at 1–100 MHz and 0.1–18 GHz was measured using an impedance analyzer (Agilent 4294A) and vector network analyzer (VNA, Agilent E8363B), respectively. The composite's core loss was measured by a wideband power analyzer (Clarke–Hess Model 2335A).

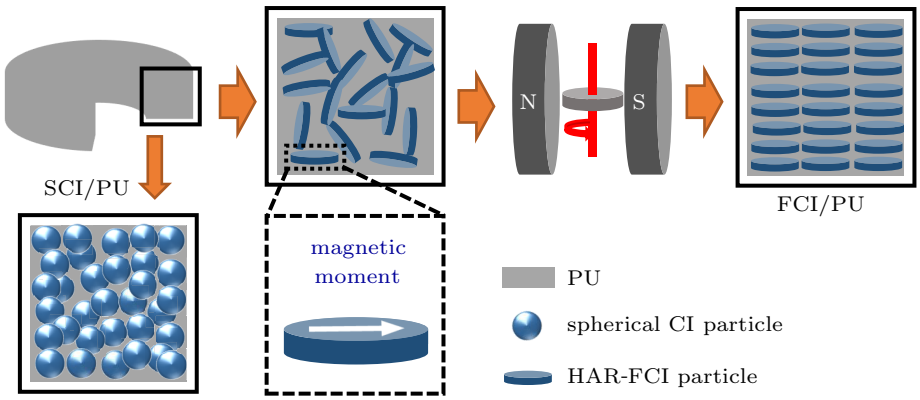


Fig. 1. Schematic diagram of the prepared FCI/PU and SCI/PU composites.

3. Results and discussion

3.1. Morphology and phase structure analysis

Figure 2 shows the morphology of R-SCI and HAR-FCI particles. Figures 2(a)–2(c) show that R-SCI particles were regular spheres in homogenous sizes, and the largest particle was approximately 5 μm. The ball-milled particles had irregular flake shapes, as shown in Figs. 2(d) and 2(e). Figures 2(f)–2(i) indicate that the diameter and thickness of the HAR-FCI particle were approximately 10 μm and 0.5 μm, respectively, so their aspect ratio was approximately 20.

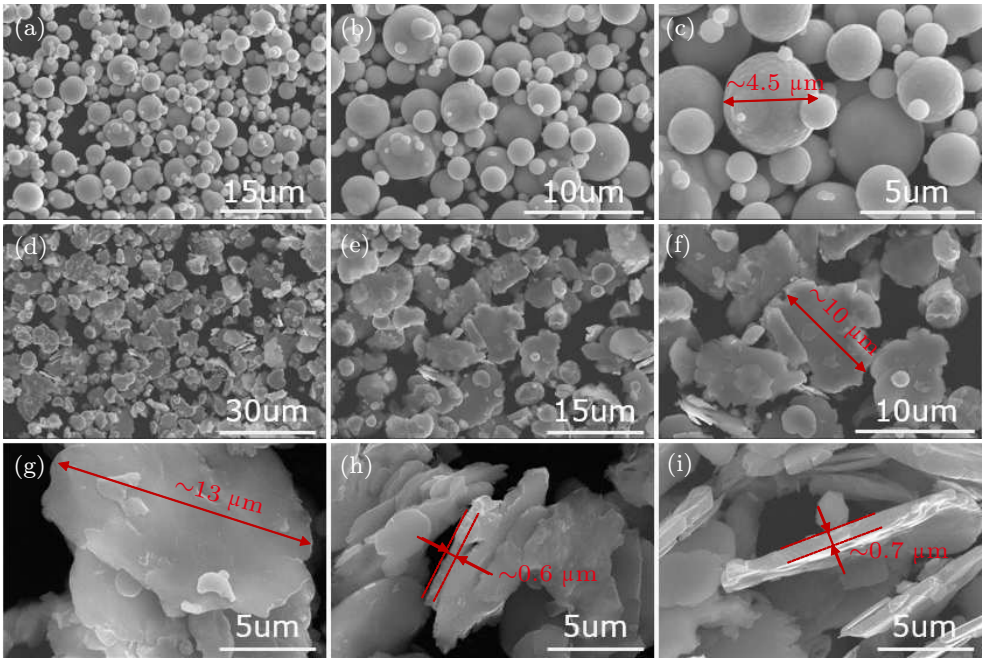


Fig. 2. Morphologies of [(a)–(c)] R-SCI and [(d), (e)] HAR-FCI particles, [(f), (g)] diameter of a single HAR-FCI particle, and [(h), (i)] thickness of a single HAR-FCI particle.

Figure 3 shows the XRD patterns of the R-SCI and HAR-FCI particles. The two sets of spectral lines were typical characteristic Fe spectra, in which the 44°, 65°, and 82° diffraction peaks correspond to (110), (200), and (211) Fe cell crystal planes with BCC structures, respectively. There are no significant changes between the two sets of peaks except a slight reduction in the diffraction peak intensity of the FAR-FCI particles. This proves that there was no phase transition during the ball milling process. The reduction in the diffraction peak intensity was mainly caused by the defects and stresses introduced during the ball milling process, which decreased the particles' crystallinity.

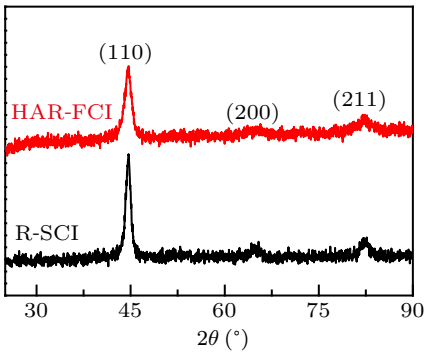


Fig. 3. XRD patterns of the R-SCI and HAR-FCI particles.

3.2. Static magnetic properties

Figure 4 shows the hysteresis loops of the FCI/PU composite in the oriented plane and perpendicular to the oriented plane, and the corresponding static magnetic parameters are presented in Table 1. For convenience, we define the composite's orientation plane as the $x0y$ plane and the direction perpendicular to this plane as the z axis. Figure 4 demonstrates that the composite was easily magnetized to saturation in the $x0y$ plane, and the corresponding magnetization saturation field was 5 kOe. In the z axis direction, however, when the external field strength reached 20 kOe, it still could not be magnetized to saturation. In addition, in the $x0y$ plane, the composite's coercive (H_c) and residual magnetization (M_r) were both significantly smaller than the z axis. This indicates that the composite's magnetic moments were distributed isotropically along the oriented plane, and the composite was more easily magnetized to saturation within the oriented plane.

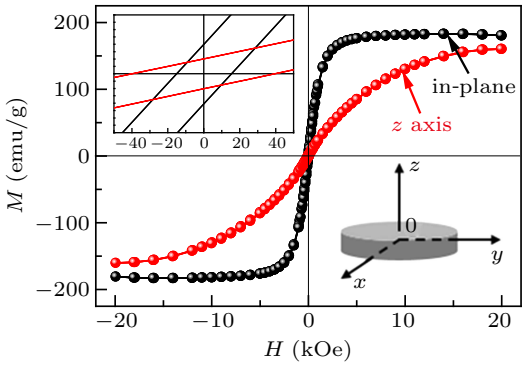


Fig. 4. Hysteresis loop of the FCI/PU composite in $x0y$ plane and z direction.

Table 1. Static magnetic parameters of the FCI/PU composite.

	H_c (Oe)		M_r (emu/g)		M_s (emu/g)
	x axis	z axis	x axis	z axis	
FCI/PU	14.9	39.6	1.85	1.02	180.5

To further study the distribution of magnetic moments in the composites, we measured the Mössbauer spectra of the

SCI/PU and FCI/PU. The γ-ray was perpendicular to the oriented plane ($x0y$ plane). We characterized the orientation degree of the composites' magnetic moment by the ratio of peaks 2 and 5 to peaks 1 and 6:[27]

$$\frac{I_{2,5}}{I_{3,4}} = \frac{4\sin^2(\theta)}{1+\cos^2(\theta)}, \tag{3}$$

where θ is the average angle between the γ-ray and magnetic moment, and $f = \sin(\theta)$ represents the magnetic moment's average orientation degree. In materials with magnetic moments completely distributed in the plane ($\theta = 90°$), the intensity ratio of the six-line spectrum should be 3:4:1:1:4:3, that is, the intensity of peaks 2 and 5 exceeds peaks 1 and 6. As shown in Fig. 5(b), the ratio of the six-line spectrum was not the typical ratio corresponding to an orientation angle $\theta = 90°$. This was mainly because some low-aspect ratio carbonyl iron particles were not completely parallel to the oriented plane during the orientation process, resulting in partial magnetic moments that were randomly arranged in the three-dimensional direction. However, Fig. 5(a) clearly shows that the intensity of peaks 2 and 5 exceeded the peaks 1 and 6. According to Eq. (3), we calculated that the orientation degrees of the two composites in the $x0y$ plane were 0.72 and 0.8, respectively. Because the HAR-FCI particles were affected by a strong demagnetizing field, their magnetic moment was bound within the plane. Combined with the hysteresis loop in Fig. 4, we can conclude that, in the FCI/PU composite, the particles rotated with the magnetic moment during the rotational orientation process and were arranged parallel to the oriented plane (except for a few carbonyl iron particles with a low aspect ratio). Due to the small anisotropic field of the HAR-FCI particles in the plane, the magnetic moment was easy to rotate in the plane, so the composite was more easily magnetized in the oriented plane, resulting in an easily magnetized plane.

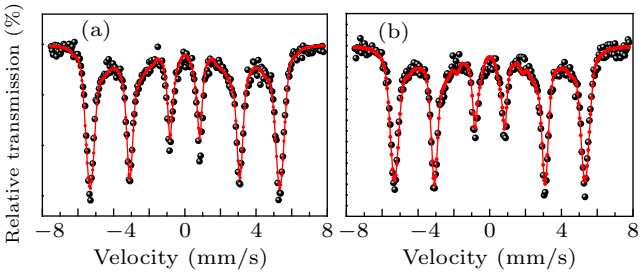


Fig. 5. Mössbauer spectrum of (a) SCI/PU and (b) FCI/PU composites.

3.3. High frequency magnetic properties

Figures 6(a) and 6(b) shows the magnetic spectra of the SCI/PU and FCI/PU composites from 1 MHz to 18 GHz. Both the composites maintained a flat permeability under 100 MHz, and the relaxation of the magnetic spectrum appeared afterward. The differences between the two composites' magnetic spectra were mainly as follows: (1) compared with the SCI/PU, the initial permeability of the FCI/PU increased by 3 times and (2) the imaginary part of the FCI/PU permeability appeared as two sets of resonance peaks. To further understand the composites' magnetization process, we fit the measured magnetic spectra. The fitting formulas are[28]

$$\begin{aligned}\mu_r' &= 1+\mu_{dw}'+\mu_{spin}' \\ &= 1+\frac{\omega_d^2\chi_{d0}(\omega_d^2-\omega^2)}{(\omega_d^2-\omega^2)^2+\alpha^2\beta^2} \\ &\quad +\frac{\chi_{s0}\omega_s^2\left[(\omega_s^2-\omega^2)+\omega^2\alpha^2\right]}{[\omega_s^2-\omega^2(1+\alpha^2)]^2+4\omega^2\omega_s^2\alpha^2},\end{aligned} \tag{4}$$

$$\begin{aligned}\mu_r'' &= \mu_{dw}''+\mu_{spin}'' \\ &= \frac{\omega_d^2\chi_{d0}\omega\beta}{(\omega_d^2-\omega^2)^2+\omega^2\beta^2} \\ &\quad +\frac{\chi_{s0}\omega_s\omega\alpha\left[\omega_s^2+\omega^2(1+\alpha^2)\right]}{[\omega_s^2-\omega^2(1+\alpha^2)]^2+4\omega^2\omega_s^2\alpha^2},\end{aligned} \tag{5}$$

where χ_{d0} and χ_{s0} represent the susceptibility contributed by domainwall displacement and magnetic moment rotation, respectively; ω_{d0} is the domainwall resonance angular frequency, ω_{s0} is the natural resonance angular frequency, β is the damping of the domainwall displacement, and α is the damping of the magnetic moment rotation. It is noted that ω_{s0} obtained by fitting here is the intrinsic resonance frequency without considering the damping effect, and the natural resonance angle frequency actually exhibited by the composite should be expressed as[28]

$$\omega_r^{spin} = \frac{\omega_{s0}}{\sqrt{1+\alpha^2}}. \tag{6}$$

Figures 6(c)–6(f) show the fitting results of magnetic spectra of the SCI/PU and FCI/PU composites. The corresponding fitting parameters are listed in Table 2. In the FCI/PU composite, a new resonance peak appeared at approximately 200 MHz. By fitting the magnetic spectra, we confirmed that this peak was derived from the domain wall resonance. This means that the SCI/PU composite was magnetized by a single magnetic moment rotation, and only natural resonance peaks existed in the magnetic spectra. During the dynamic magnetization process, however, the easy plane-like FCI/PU composite contained contributions of both the magnetic moment rotation and domain wall displacement.[29] In addition, compared with the SCI/PU, the composite's permeability increased by 3 times (from 7.5 to 21.5) at 100 MHz and its natural resonance frequency (f_r) shifted to higher frequencies by 1.7 GHz. The simultaneous increases of μ_i and f_r led to an obviously increased $(\mu_i - 1) f_r$ value (5.1 times), which is important for the composite to break through the Snoek limit and to work efficiently at higher frequencies.

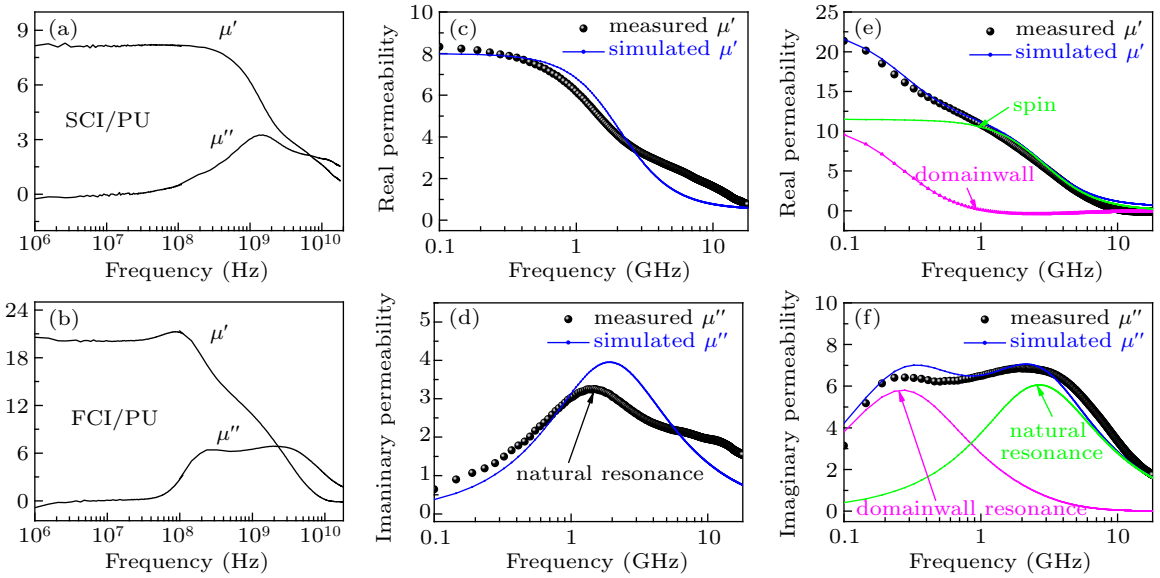


Fig. 6. [(a), (b)] Permeability of the SCI/PU and FCI/PU at 1 MHz–18 GHz, [(c), (d)] fitting permeability of the real and imaginary parts of the SCI/PU composite, and [(e), (f)] fitting permeability of the real and imaginary parts of the FCI/PU composite.

Table 2. Relevant parameters corresponding to the fitting magnetic spectra of the SCI/PU and FCI/PU composites.

	Domainwall displacement			Spin rotation		
	χ_{do}	ω_d	β	χ_{so}	ω_s	α
SCI/PU				7.5	3.8×10^{10}	4
FCI/PU	11	6.9×10^{9}	3×10^{10}	11.5	5.3×10^{10}	3

3.4. Core loss

The test of core loss is carried out at room temperature. When core loss is tested, the composite needs to be wound and a certain voltage (V_{RMS}) is applied to ensure that the inner part of the composite reaches a desired B_m. According to B_m, the V_{RMS} can be given as follows:

$$V_{RMS} = 4.44NA_eB_mf, \tag{7}$$

where N is the number of coil turns, and A_e is effective sectional area:

$$A_e = \frac{h(\ln\frac{D}{d})^2}{|\frac{2}{D}-\frac{2}{d}|}. \tag{8}$$

The effective volume (V_e) formula of the composite is as follows:

$$V_e = \frac{2\pi h(\ln\frac{D}{d})^3}{(\frac{2}{D}-\frac{2}{d})^2}, \tag{9}$$

where D and d are the outer diameter and inner diameter, and h is the thickness of the magnetic ring.

Figures 7(a) and 7(b) show the core loss of the SCI/PU and FCI/PU at 50–500 kHz for the magnetic fluxes of 10, 20, and 30 mT, respectively. The composites' core loss increased slowly with the frequency. Figure 7(a) shows that, at 500 kHz, the core losses at 10, 20, and 30 mT for the SCI/PU were 191.7, 804.2, and 1912.6 mW/cm^3, respectively, while the core losses of the FCI/PU under the same conditions were 80.0, 355.3, and 810.7 mW/cm^3, as demonstrated in Fig. 7(b).

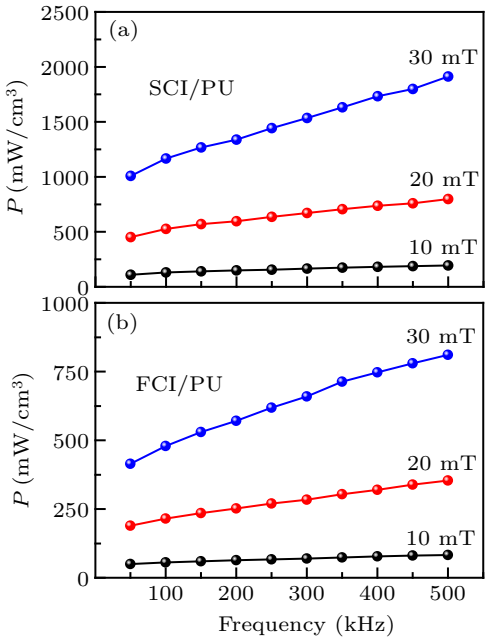


Fig. 7. The variation trend of coreloss with frequency for (a) SCI/PU and (b) FCI/PU under the magnetic fluxes of 10, 20, and 30 mT.

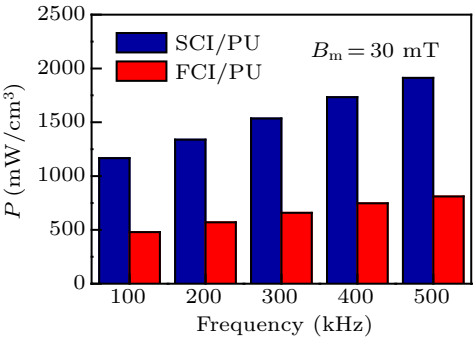


Fig. 8. Histogram of coreloss comparison for SCI/PU and FCI/PU at 30 mT.

Figure 8 shows a histogram of the core loss comparison of the SCI/PU and FCI/PU at 30 mT. The core loss of the FCI/PU

significantly declined in comparison to the SCI/PU. Under the same conditions, the core loss of the FCI/PU decreased by approximately 60%.

4. Conclusions

To break through the Snoek limit and to obtain a higher permeability at higher frequencies, we have used HAR-FCI particles to prepare an FCI/PU composite with an easy plane-like structure. The composite's dynamic magnetization process and core loss are carefully studied, leading to the following conclusions:

(1) Due to its easy-plane-like structure, the $(\mu_i - 1) f_r$ value of the FCI/PU composite increases by 5.1 times compared with the SCI/PU. This effectively breaks through the Snoek limits, demonstrating that the composite can work efficiently at higher frequencies.

(2) The FCI/PU composite has a domain wall resonance peak at 200 MHz, which shows that both the domain wall displacement and magnetic moment rotation occur simultaneously during the FCI/PU's dynamic magnetization process.

(3) Compared with the SCI/PU, the core loss of the FCI/PU under the same conditions decreases by nearly 60%.

References

[1] Silveyra J M, Ferrara E and Huber D L 2018 *Science* **362** eaao0195
[2] Wu C, Huang M Q, Luo D H, Jiang Y Z and Yan M 2018 *J. Alloys Compd.* **741** 35
[3] Chen Y, Zhang L, Sun H S, Chen F F, Zhang P, Qu X H and Fan E D 2020 *J. Alloys Compd.* **813** 152205
[4] Zhou B, Dong Y Q, Liu L, Chang L, Bi F Q and Wang X M 2019 *J. Magn. Magn. Mater.* **474** 1
[5] Mori S, Mitsuoka T, Sonehara M, Saoto T and Matsushita N 2017 *AIP Adv.* 056657
[6] Waide P and Brunner C U 2011 *International Energy Agency (IEA)* working paper: *Energy-efficiency policy opportunities for electric motor-driven systems*
[7] Iacopi F, Van Hove M, Charles M and Endo K 2015 *MRS Bull.* **40** 390
[8] Wang S F, Chiang Y J, Hsu Y F and Chen C H 2014 *J. Magn. Magn. Mater.* **365** 119
[9] Ahmed M A, Rady K E and Shams M S 2015 *J. Alloys Compd.* **622** 269
[10] Liu D, Chen X P, Ying Y, Zhang L, Li W C, Jiang L Q and Che S L 2016 *Ceram. Int.* **42** 9152
[11] Waqas H, Qureshi A H, Subhan K and Shahzad M 2012 *Ceram. Int.* **38** 1235
[12] Sun K, Lan Z W, Yu Z, Li L Z, Huang J M and Zhao X N 2008 *J. Phys. D: Appl. Phys.* **41** 235002
[13] Sun K, Pu Z Y, Yang Y, Chen L L, Yu Z, Wu C J, Jiang X N and Lan Z W 2016 *J. Alloys Compd.* **681** 139
[14] He X M, Yan S M, Li Z W, Zhang X, Song X Y, Qiao W, Zhong W and Dou Y W 2015 *Chin. Phys. B* **24** 127502
[15] Liu D, Gao S M, Jin R C, Wang F, Chu X X, Gao T P and Wang Y B 2019 *Chin. Phys. B* **28** 057503
[16] Zhou X, Hou Z L, Li F and Qi X 2010 *Chin. Phys. Lett.* **27** 117501
[17] Li W C, Cai H W, Kang Y, Ying Y, Yu J, Zheng J W, Qiao L, Jiang Y and Che S L 2019 *Acta Mater.* **167** 267
[18] Liu D, Wu C, Yan M and Wang J 2018 *Acta Mater.* **146** 294
[19] Zhou B, Chi Q, Dong Y Q, Liu L, Zhang Y Q, Chang L, Pan Y, He A, Li J W and Wang X M 2020 *J. Magn. Magn. Mater.* **494** 165827
[20] Zhang L R, Lv H, Liu X, Bai J M and Wei F L 2012 *Chin. Phys. B* **21** 037502
[21] Li W C, Zuo T L, Liu X H, Wei Q Q, Zhou X Y and Yao D S 2015 *Chin. Phys. B* **24** 047503
[22] Luo Z Y, Tang J, Ma B, Zhang Z Z, Jin Q Y and Wang J P 2012 *Chin. Phys. Lett.* **29** 127501
[23] Yao D S, Ge S H, Zhou X Y, Zhang B M and Zuo H P 2010 *Chin. Phys. Lett.* **27** 067502
[24] Snoek J L 1947 *Nature* **160** 90
[25] Snoek J L 1948 *Physica* **14** 207
[26] Xue D S, Li F S, Fan X L and Wen F S 2008 *Chin. Phys. Lett.* **25** 4120
[27] Haggstrom L, Grinasl L, Wappling R and Devanarayanan S 1973 *Phys. Scr.* **7** 125
[28] Tsutaoka T 2003 *J. Appl. Phys.* **93** 2789
[29] Liu X, Wu Peng, Wang P, Wang T, Qiao L and Li F S 2020 *Chin. Phys. B* **29** 077506